Visible light emission from thin films containing Si, O, N, and H

B. H. Augustine[a] and E. A. Irene[b]
Department of Chemistry CB No. 3290, University of North Carolina at Chapel Hill, Chapel Hill, North Carolina 27599-3290

Y. J. He,[c] K. J. Price, and L. E. McNeil
Department of Physics and Astronomy CB No. 3255, University of North Carolina at Chapel Hill, Chapel Hill, North Carolina 27599-3255

K. N. Christensen and D. M. Maher
Department of Materials Science and Engineering, North Carolina State University, Raleigh, North Carolina 27695

(Received 20 February 1995; accepted for publication 31 May 1995)

We report the fabrication, chemical, optical, and photoluminescence characterization of amorphous silicon-rich oxynitride (SiO_xN_y:H) thin films by plasma-enhanced chemical-vapor deposition. The film compositions were followed by changes in the refractive index. X-ray photoelectron and Fourier transform infrared spectroscopy indicate that the chemical composition is dominated by silicon suboxide bonding with N present as a significant impurity. A broad tunable photoluminescence (PL) emission is visible at room temperature with a quantum efficiency of 0.011% at peak energies to 3.15 eV. The radiative lifetimes are less than 10 ns, and there is nearly no temperature dependence of the PL intensity down to 80 K. *Ex situ* annealing at temperatures above 850 °C results in an increase in PL efficiency by nearly three orders of magnitude, and the PL intensity is independent of the annealing ambient. The PL results are remarkably similar to literature results in oxidized porous silicon and oxidized nanocrystalline Si thin films, and suggest that the radiative center is due to the defect structure in the silicon suboxide moiety. © *1995 American Institute of Physics.*

I. INTRODUCTION

Recently there has been considerable research effort in the study of light emission from silicon-based materials. The technological drive derives from the desire to integrate optoelectronic devices with silicon-based microelectronics technologies. Scientifically, there has been a desire to understand the nature of light emission from an indirect-band-gap material such as Si. Much of the early work focused on the concept of "band-structure engineering" through Brillouin zone-folding effects using alternating multiple-quantum-well (MQW) layers of Si and Ge.[1,2] Another approach has been through isoelectronic impurity doping of rare-earth ions such as Er^{+3} into the crystal silicon lattice.[3] Both of these approaches lead to emission in the near-infrared spectral region, but to date have only met with limited success in terms of high quantum efficiency at room temperature.

More recently however, the attention has shifted to electrochemically etched crystalline silicon known as porous silicon (PSi),[4] due to the intense room-temperature photoluminescence (PL) in the visible spectral region, and the ease of fabrication. This work has spawned research on silicon nanoparticles,[5] films of nanocrystalline silicon imbedded in SiO_2,[6] crystal silicon remnants in the SiO_2 glass-melt reaction,[7] recrystallization of amorphous silicon,[8] and Si^+ ion implantation into fused silica,[9] among many others. Each of these distinct preparation techniques has in common crystalline silicon in nanometer size scales and reports intense visible room-temperature PL. Yet, another approach to silicon-based emission is through thin films of hydrogenated amorphous silicon (a-Si:H), and a-Si:H–based alloys such as a-SiO_x:H, a-SiN_x:H, and a-SiC_x:H.[10–14] These materials exhibit several important luminescent properties. The first is that low-defect-density a-Si:H has nearly 30% quantum efficiency at 77 K.[15] However, the PL intensity decreases by nearly four orders of magnitude at room temperature. The second is that the peak energy for a-Si:H PL is in the near-infrared (NIR) spectral region at 1.3 eV. This emission can be tuned into the visible spectral region in amorphous silicon-based alloys by varying the composition of the alloys. This tuning is due to the changing band gap with changing chemical composition.[11–14] With all of these distinct approaches to light emission in silicon-based materials in the literature, it is unclear how these materials and methods compare to one another in terms of quantum efficiency and technological significance. Also, there is continued disagreement in the identification of the chemical moiety responsible for the PL.

In order to address some of these issues, we have prepared various amorphous silicon oxynitride (a-SiO_xN_y:H) thin films by the plasma-enhanced chemical-vapor-deposition (PECVD) technique. Prior to the presentation of the PL results, we address materials characterization, so that the luminescence results can be interpreted in terms of the materials properties. We show that these materials exhibit tunable visible PL of comparable intensity and energy to PSi at room temperature after appropriate postdeposition anneal-

[a]Present address: MCNC Electronic Technologies Division, 3021 Cornwallis Rd., Research Triangle Park, NC 27709.
[b]Electronic mail: gene_irene@unc.edu
[c]Present address: Lighting Research Center, Rensselear Polytechnic Institute, Troy, NY 12180.

 0021-8979/95/78(6)/4020/11/$6.00

TABLE I. Series I and series II samples used in this study.

Sample number	N_2O:SiH_4	As deposited		Annealed in N_2 (1050 °C)		Deposition rate (nm/min)
		Refractive index	Thickness (nm)	Refractive index	Thickness (nm)	
I-a	5.0	$1.475-0.00i$	117.0	$1.482-0.00i$	120.2	24.63
I-b	4.0	$1.509-0.00i$	121.3	$1.516-0.00i$	117.8	16.73
I-c	3.0	$1.590-0.00i$	108.4	$1.597-0.00i$	102.6	9.86
I-d	2.5	$1.642-0.00i$	106.6	$1.649-0.00i$	100.3	7.75
I-e	2.0	$1.702-0.00i$	106.1	$1.710-0.00i$	100.0	6.43
I-f	1.5	$1.778-0.00i$	102.7	$1.784-0.00i$	97.7	5.20
I-g	1.0	$1.861-0.00i$	91.7	$1.885-0.00i$	87.7	3.99
II-a	5.0	1.470	193.0			
II-b	2.5	1.697	259.9			
II-c	1.0	1.841	303.3			
II-d	1.95	1.61	605			

ing. The PL properties of peak energy and radiative lifetime are similar to oxidized porous Si,[16] and the materials characterization helps to identify the chemical species that are important for the photoluminescence properties of these materials.

II. EXPERIMENTAL CONDITIONS

We have prepared different compositions of a-SiO_xN_y:H thin-film materials by PECVD through the reaction of SiH_4 and N_2O at elevated temperatures. Silicon-rich material is obtained by increasing the SiH_4:N_2O ratio such that there is excess SiH_4 in the reaction region.[17] Changing compositions are followed by observing changes in the refractive index of the films, which can be modeled with an effective medium approximation such as that described by Bruggemann.[18,19] In addition to Si—O bonding, N and H bonds are present in these PECVD films, albeit in lower concentrations than for Si—O. Both the excess Si and the Si—N bond contribute to a higher refractive index N in the films relative to stoichiometric SiO_2 ($N=1.465-0.0i$). Materials characterization includes single wavelength ellipsometry (SWE), x-ray photoelectron spectroscopy (XPS), Fourier transform infrared spectroscopy (FTIR), optical-absorption spectroscopy, and transmission electron microscopy (TEM).

We have performed two distinct series of experiments on the silicon-rich oxides. In the first series of samples, labeled I-a through I-g in Table I, the films were grown to near one-half an ellipsometric period $d_{1/2}$, as determined by the following equation:

$$d_{1/2}=\frac{\lambda}{4}\,(n_{\text{film}}^2-\sin^2\,\phi)^{-1/2},$$

where λ is the HeNe laser wavelength of 632.8 nm, n_{film} is the real component of the refractive index of the film, and ϕ is the angle of incidence of the ellipsometer, which is 70.0° for this study. The deposited films range in refractive index from $N=1.475-0.0i$ to $N=1.885-0.0i$ as determined by null ellipsometry. At half of an ellipsometric period, the measurement is most sensitive to both the film index and thickness. This series of films were grown to determine the dependence of the PL peak energy on the silicon content as monitored by ellipsometry. The second series of films, labeled II-a through II-d and also listed in Table I, consisted of 200–600-nm-thick films with refractive indices ranging from $N\approx 1.47-0.0i$ to $1.84-0.0i$. These thicker films were used to examine the PL behavior with different annealing conditions, and to perform various spectroscopies.

All films were deposited in a standard parallel-plate geometry PECVD system operating at 13.56 MHz. The deposition conditions were identical, except for SiH_4:N_2O flow ratios and deposition times. Reaction conditions were as follows: forward plasma power was 35±3 W, pressure was 100.0 mTorr, SiH_4 flow rate was 20 sccm, and substrate temperature was 300 °C. The gases were very large scale (VLSI) grade 5% SiH_4 in He carrier gas, and VLSI grade 100% N_2O. The substrates were ⟨100⟩ p-type c-Si wafers, sapphire wafers, or roughened quartz slides that had received a slightly modified RCA cleaning.[20] In addition, the Si wafers were dipped in 49% HF for 10 s to remove any surface native oxide, rinsed in de-ionized (DI) water (11 MΩ cm) for 5 s, dried in N_2, and immediately placed under vacuum in the deposition chamber.

The annealing studies consisted of *ex situ* thermal annealing at atmospheric pressure in a fused-silica tube furnace with flowing ambient gases. Annealing ambients consisted of O_2, forming gas (5% H_2/95% N_2), dry N_2, and Ar. A rapid thermal anneal (RTA) in vacuum was also performed. Anneal temperatures were varied up to 1050 °C. All of the films demonstrated an increase in refractive index and a decrease in thickness upon annealing, indicating densification.

Time-independent photoluminescence measurements were performed using a double-grating 0.85 m monochromator instrument, predominantly with the 488.0 nm (2.54 eV) line from a continuous-wave (cw) Ar^+ laser, and a GaAs photomultiplier tube in the photon counting mode. PL was also performed with other cw Ar^+-ion laser lines, and with the 442 nm (2.80 eV) and 325 nm (3.82 eV) lines from a cw HeCd laser. Low-temperature PL was performed in a Joule–Thompson cryostat at 80 K. The quantum efficiency was determined at room temperature by comparing the emission from the thin films with the known quantum efficiency of a 25 μm ruby sphere at the 488 nm excitation wavelength

under identical collection conditions. Time-resolved PL was performed using the 335 nm output from a pulsed N_2 laser with a pulse-width of 400 ps and a 3 Hz repetition rate. The N_2 laser then pumped a dye laser using Excelite dye with an output wavelength of 376 nm. Detection was performed with a fast GaAs photomultiplier tube and recorded on a transient digitizer. The overall instrument response time is on the order of 5–10 ns.

XPS was performed on samples I-a, I-c, I-e, and I-g. A monochromatic x-ray source with a resolution of 1.2 eV full width at half-maximum (FWHM) was used (Al $Ka_{1,2}$ $h\nu$ =1486.6 eV) to reduce the spectral broadening in the XPS study. The sample plane was tilted 65° with respect to the analyzer input, which yields an electron escape depth of about 50 Å, so the technique only probes the near surface of the samples and not the bulk. Depth profiling was not performed on any of the samples except for the most silicon-rich sample (I-g after annealing) because large modifications of the film composition are expected due to preferential sputtering effects.

FTIR was performed on samples II-a–II-c which were deposited on double-side-polished c-Si wafers to reduce optical scatter. In addition to bonding information, optical-absorption data were measured in the 190–900 nm wavelength range using samples deposited on roughened fused silica substrates to avoid optical interference effects. Samples were deposited simultaneously so the thickness and index of the FTIR and absorption samples are identical despite the different substrates. Each spectroscopic technique was performed on samples both as deposited and after annealing. Morphology was determined on selected samples by TEM.

III. a-SiO_xN_y:H FILMS MATERIALS CHARACTERIZATION

A. FTIR

Philipp has presented a random-bonding model to describe the optical properties of the amorphous SiO_x system.[21] This model suggests that all compositions between Si and SiO_2 are possible, and that the atoms are blended on an atomic scale, i.e., SiO_x does not necessarily consist of simple mixtures of pure Si and SiO_2. The silicon bonding continues to be tetrahedral and statistical, which can be described by Si-(Si_xO_{4-x}). While this model is not universally accepted, it is used here to interpret the spectroscopic results on the a-SiO_xN_y:H films described below.

In both the XPS and FTIR spectroscopies, the primary trend after postdeposition annealing is toward more SiO_2-like bonding in the films; however, it appears that annealing does not simply continue to oxidize the silicon suboxide moieties which are present in the as-deposited films. Figure 1(a) shows the FTIR results of the as-deposited films, and Fig. 1(b) shows the results after annealing in N_2 at 1050 °C for 30 min. The dominant feature in these spectra is the broad Si–O–Si asymmetric stretching vibrational resonance, which occurs at 866, 973, and 1050 cm^{-1} with decreasing refractive index in the films from samples II-c–II-a. This peak has been reported[22] in suboxide materials to vary nearly linearly from 1075 cm^{-1} for stoichiometric thermal oxide (108 cm^{-1}

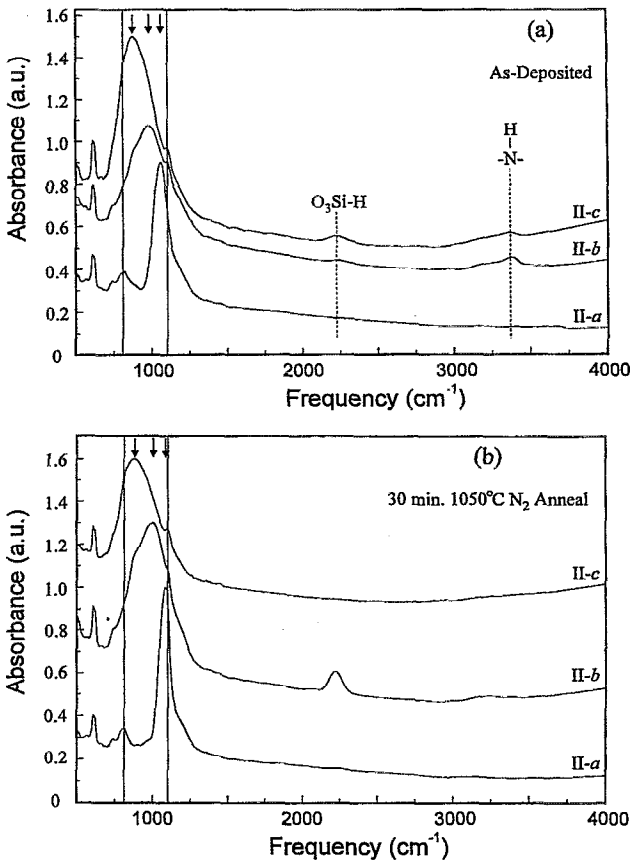

FIG. 1. Transmission Fourier transform infrared spectra of a-SiO_xN_y:H thin films (500 scans at 8 cm^{-1} resolution). (a) shows the samples as deposited and (b) shows the same samples after a 30 min anneal in dry N_2 at 1050 °C. The spectra are labeled by the sample numbers II-a–II-c. Vertical solid lines indicate the vibrational asymmetric stretching frequency of stoichiometric SiO_2 and Si_3N_4 at 1075 and 804 cm^{-1}, respectively. The vertical dashed lines indicate the vibrational frequencies of the O_3Si—H and ═N—H bonding at 2250 and 3340 cm^{-1}, respectively. Vertical arrows designate the peak positions of the asymmetric vibrational mode in each sample.

FWHM), to 945 cm^{-1} for pure a-Si with oxygen impurities present. Stoichiometric SiO has a vibrational frequency of 985 cm^{-1}.[23] In sample II-a the dominant resonance is due to Si—O bonding as evidenced by both the asymmetric stretch at 1050 cm^{-1} and the separate lower-frequency absorption at 800 cm^{-1} due to the rocking mode in bridging Si—O—Si bonds. The position of the stretching resonance in the other two samples appears to be noticeably influenced by the presence of Si–N as well as suboxide bonding. The primary Si–N stretching frequency is at 804 cm^{-1}, and has been reported[24] to monotonically shift and broaden in oxynitride materials between the two extremes of stoichiometric Si_3N_4 and SiO_2. Sample II-c contains a significant percentage of Si—N bonding since the frequency of the peak is at 866 cm^{-1}, which is lower than a-Si with O_2 impurities present at 945 cm^{-1}. There is a small shoulder which develops at 804 cm^{-1} in both samples II-b and II-c, compared to a separate resonance for sample II-a. An additional feature of the Si–O or Si–N resonance is a broadening of the peak, which is indicative of chemical disorder, strain, or different bonding geometries at the atomic level. The FWHM of the peaks are

240, 284, and 112 cm^{-1} for the as-deposited samples II-c, II-b, and II-a, respectively. There are few dramatic changes in the spectra after annealing. Each shows a trend toward more stoichiometric SiO_2-like bonding, but the changes in frequency and width are subtle.

There are several other IR spectral features which are present in these samples. There are weak absorptions due to Si—H bonding which occur between 2220 and 2240 cm^{-1} as deposited in samples II-b and II-c. This resonance has been attributed a Si—H bond with three bridging oxygen atoms back-bonded to the Si atom.[25] Estimating from the intensity of these peaks, the amount of bonded O_3Si–H is less than 5 at. %, since the detection limit in FTIR is about 0.5 at. % for Si–H. After annealing at 1050 °C in N_2, sample II-b shows a dramatic increase in bonded Si–H, but the other two samples show little or no evidence of Si–H within the detection limit of the technique. This behavior is puzzling because one might expect the high-temperature anneal to drive out the hydrogen, since it is well established that temperatures above 580 °C are sufficient to completely desorb H_2 from a hydrogen-passivated silicon surface.[26] The low hydrogen concentration as deposited is also puzzling considering that PECVD processes are known to generate large Si—H bonding concentrations; however, Pai, *et al.*[27] have shown that high He dilution decreases the number of Si—H bonds present in PECVD SiO_x deposition. With the flow rates of N_2O below 5 sccm and a 95% dilution of SiH_4 with He, the deposition environment is heavily He diluted. This gives rise to the favorable condition of Si–O–Si linkages rather than Si–H termination or Si—OH bonding.

Another broad resonance is observed in the as-deposited films of samples II-b and II-c between 3200 and 3350 cm^{-1}. This peak is due to N—H bonds bridging the silicon network.[28] This peak disappears after annealing, which is consistent with H_2 release from the Si–N–Si linkage at high temperature. It should be noted that there is no IR evidence of a broad resonance at frequencies of 3400–3700 cm^{-1} either as deposited or after annealing which would be due to O—H bonding as terminated Si–OH or H_2O in the films. A final spectral feature at 608 cm^{-1} is an artifact due to the silicon substrate.

B. X-ray photoelectron spectroscopy

XPS was used to examine the core-level bonding, particularly the Si $2p$ region, in several of the samples which spanned the range of refractive index from nearly stoichiometric SiO_2 in sample I-a, to the most silicon-rich sample, I-g. The Si $2p$ region occurs at binding energies from about 98 to 104 eV, which is shown in Fig. 2 for each of the samples as deposited and after annealing at 1050 °C in N_2 for 30 min. With increasing O addition to the film, the oxidation state of the silicon gradually changes from Si^0, for pure amorphous silicon bonded to four nearest-neighbor silicon atoms, to Si^{4+} for fully oxidized amorphous SiO_2, i.e., a silicon atom bonded to four nearest-neighbor oxygen atoms. The increasing electronegativity of the Si—O bond relative to the Si—Si bond results in a shift to higher binding energy of the core-level electrons in the silicon.[23] The binding energies for this progression range from approximately 99.0 to

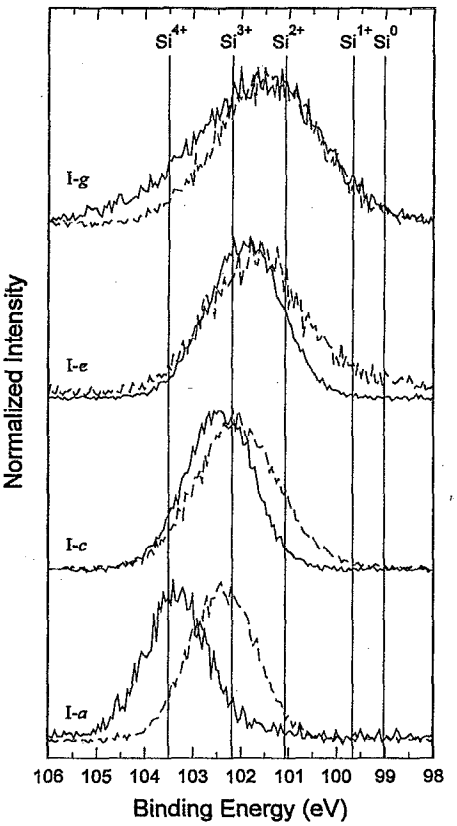

FIG. 2. Si $2p$ region from x-ray photoelectron spectroscopy of samples I-(a,c,e,g) using a monochromatic x-ray source (Al $K\alpha_{1,2}$ $h\nu$=1486.6 eV, theoretical broadening 1.2 eV). The solid lines are the XPS signal after a 30 min anneal in dry N_2 at 1050 °C, and the broken lines are the signal as deposited. No sputtering has been performed except for sample I-g after annealing, which received an Ar^+ sputter for 1.5 min. The solid vertical lines are literature values for the silicon oxidation states at 99.0, 99.6, 101.1, 102.2, and 103.5 eV for the Si^0, Si^{1+}, Si^{2+}, Si^{3+}, and Si^{4+} oxidation states, respectively. Peaks have been normalized, and charge corrected using the adventitious C peak at 285 eV.

103.5 eV with increasing oxide character. We have used the literature values of the binding energies assigned to the intermediate oxidation states by Rochet *et al.*[23] The Si^{1+}, Si^{2+}, Si^{3+}, and Si^{4+} oxidation states are represented in Fig. 2 as vertical lines with binding energies equal to 99.6, 101.1, 102.2, and 103.5 eV, respectively.

Each of the samples showed sample charging. Hence, the spectra in Fig. 2 were corrected for the charging effect by using the literature value of the adventitious C peak at 285.0 eV, and adjusting each spectrum accordingly.[29] Two trends emerge with increasing refractive index in the films. The first trend is a shift toward lower binding energy with increasing refractive index, which suggests that a large fraction of the silicon atoms in the higher-index films are present in suboxide oxidation states. For example, sample I-c ($N=1.60-0.0i$) appears to have predominantly Si^{3+}-type bonding as deposited, while the sample I-e ($N=1.70-0.0i$) peak has shifted to lower binding energy, indicating a bonding type between Si^{3+} and Si^{2+}. The second trend that emerges is an increase in FWHM with increasing refractive index. Table II shows the binding energy and width of each of the samples, along with a stoichiometric thermal SiO_2 sample using the

TABLE II. Summary of XPS results. Totals may not add up to 100% because of adventitious C which was present but not listed.

	As deposited					Annealed in N_2 (1050 °C)				
Sample number	Binding energy (eV)	FWHM (eV)	% Si	% N	% O	Binding energy (eV)	FWHM (eV)	% Si	% N	% O
I-a	102.40	1.72	27.8	1.0	62.3	103.40	1.51	30.6	1.5	54.4
I-c	102.05	1.84	29.7	11.3	50.5	102.55	1.64	29.3	10.6	49.8
I-e	101.60	1.91	31.2	20.0	36.7	102.15	1.82	31.3	17.9	41.9
I-g	101.55	2.31	34.2	23.8	32.0	101.15	3.03	39.2	20.2	39.4
					Thermal					
SiO_2	103.35	1.55	30.6		59.9					

same instrument conditions. All of the samples, except the annealed sample I-a, have a larger peak width than the reference thermal SiO_2 sample, indicating more than one oxidation state present for the PECVD films. The theoretical broadening due to the instrument is only 1.2 eV, while all the peaks all have FWHM of greater than 1.5 eV. We did not attempt to fit Gaussian components for each of the silicon suboxide states, but use the literature binding energy values only as a qualitative reference.

Upon annealing the samples two trends emerge: The peak positions move toward higher binding energy and the peak widths narrow. The first observation suggests that the films are tending toward more stoichiometric SiO_2-like character, which is concordant with the FTIR results notwithstanding that XPS is only a near-surface probe. As alluded to earlier, it was necessary to perform depth profiling on sample I-g after annealing. This sample showed nearly stoichiometric SiO_2 bonding by XPS near the surface despite a high bulk refractive index. Ar^+ ion sputtering was performed for 1.5 min to yield the spectrum shown in Fig. 2 indicating that, indeed, the near surface had oxidized while the bulk remained in a lower oxidation state. Again, this procedure was avoided to prevent preferential sputtering effects, but suggests that, if anything, the reported binding energies in Fig. 2 are too high and underestimate the silicon suboxide bonding contribution. The narrowing of the peaks suggests that the films are becoming more ordered chemically. In fact, sample I-a after annealing is nearly identical to the thermal oxide sample, as the similarity in refractive index would suggest.

An important point to note is that we do not observe phase separation into Si^0 and SiO_2 after annealing according to the reaction

$$2SiO \rightarrow SiO_2 + Si^0,$$

despite the fact that SiO_x is predicted to be thermodynamically unstable at temperatures of 1050 °C. Other reports follow the phase separation reaction with XPS by observing a peak at 103.5 eV due to SiO_2 and at 99.0 eV due to Si^0.[17,23,30,31]

An additional complication arises from the fact that the material is not simply a-SiO_x, as was demonstrated by FTIR in Sec. III A. There is also a significant contribution due to Si—N bonding present in the films. Table II lists the atomic concentrations of the Si, O, and N present by comparing the peak intensities from the XPS, and using the instrumental sensitivity factors for each element. One can see that N is present as a significant component in each of the samples except for sample I-a, with nitrogen contributions up to 25%±5% in sample I-g. The binding energy of the Si—N bond is at approximately 102.0 eV, which is consistent with the idea that silicon bonded to the less electronegative nitrogen will have a lower binding-energy oxidation state in Si_3N_4 than SiO_2. Unfortunately, XPS peaks due to silicon suboxide and silicon nitride cannot be distinguished from one another, so Fig. 2 shows a superposition of the oxidation states of silicon due to both SiO_x and SiN_x bonding.

We believe that most of the nitrogen is present as an interstitial in the SiO_x from the plasma reaction, rather than in the form of Si_3N_4, because the nitrogen concentration in the film determined by XPS is not sufficient to account for the magnitude of the refractive index. For example, sample I-g after annealing has a refractive index of $N=1.885-0.0i$. Using the Bruggeman effective medium approximation[18,19] (BEMA) to model the volume fraction in the film, one finds that a two-component mixture of stoichiometric SiO_2 ($N=1.465-0.0i$) and SiN:H ($2.000-0.0i$) would yield components of 21% SiO_2 and 79% SiN:H. This is clearly not the case from XPS, which suggests a volume fraction of Si—N bonds of ~25%. The remainder of the magnitude of the refractive index must be derived from suboxide bonding in the silicon-rich oxide.

C. Optical-absorption spectroscopy

Optical-absorption spectroscopy was performed on samples II-a–II-c deposited on roughened quartz slides in the wavelength range of 190–900 nm. The commonly cited optical gap determined by the Tauc method was not found because the expression $(\alpha h\nu)^{1/2}$ vs $h\nu$ did not yield a linear fit over at least 1 decade. This has been observed in other amorphous dielectric materials,[14] and as such we report the E_{04} optical gap, which is the energy at which the absorption coefficient α is equal to 10^4 cm^{-1}. Since the samples are quite thin, optical interference effects were evident despite the roughened quartz substrate and, hence, the value of E_{04} can only be considered an estimate.

It was found that only sample II-c, with the highest refractive index, had an E_{04} gap in the visible spectral region at

2.8 eV as deposited. Sample II-b had an E_{04} optical gap greater than 5 eV, and sample II-a had an optical gap greater than the instrument range of 7 eV. Interestingly, the E_{04} gap displayed a large red shift of about 0.3 eV in sample II-c after annealing at 950 °C for 30 min in N_2. The lower index samples exhibited smaller, but measurable, red shifts as well. While these samples did not appear to have phase separated based on the TEM and XPS measurements, the optical properties attributable to Si—Si bonding become more evident after annealing. This is corroborated by the increase in refractive index upon annealing. The value of the optical gap enables comparison with Philipp's work on amorphous SiO_x and SiN_x materials,[21,32] and suggests an approximate composition for these thin films. From this comparison, the high-index films are close to SiO, which has an E_{04} equal to ~2.5 eV, while the lower-index films have a composition, $x>1.5$, and probably closer to 1.8 considering the large optical gap.

D. Morphology results

TEM was performed on samples I-a, I-c, and I-g. High-resolution cross-sectional TEM revealed no evidence for crystallinity in the films either as deposited or after annealing. This observation confirmed the XPS results in Sec. III B that the materials did not phase separate into nanocrystalline Si(nc-Si) and SiO_2 after annealing, and remain an entirely amorphous material. The possibility of nanocrystallites is not entirely ruled out by TEM because the total sampling volume in cross-sectional TEM is very small. However, if there are nanocrystallites present, they must be smaller than 2 nm with a small total volume fraction in the films, a possibility which is unlikely considering the XPS results.

IV. PHOTOLUMINESCENCE RESULTS

All of the as-deposited films show weak room-temperature (RT) PL in the visible spectral region, with a peak at about 2.2 eV when excited by the 488 nm (2.54 eV) line from an Ar^+-ion laser, except for the stoichiometric oxide sample which showed no PL within the detection limit of the instrument. After postdeposition annealing at temperatures >850 °C, the RT PL intensity increases by nearly three orders of magnitude, and the peak position of the PL varies with composition. To our knowledge, this is the first report of the PL intensity continuing to improve with high-temperature annealing in a-SiO_x:H or a-SiN_x:H materials. Others[33,34] have reported an initial increase of PL intensity up to 400–500 °C, followed by a rapid falloff in intensity at higher temperatures. This has been explained by an increase in the dangling bond density, presumably by the release of H_2 from the amorphous matrix at high temperatures.

The RT PL results for series I samples in Fig. 3 show the effect of varying the refractive index on PL peak position and intensity. All of these samples were annealed at 1050 °C in a dry N_2 ambient for 30 min. The peak energy red shifts from 2.30 eV to nearly 2.05 eV with increasing refractive index. It is interesting to note, however, that the peak shift saturates for the middle index samples at a refractive index of $N=1.60-0.0i$, and then continues to blue shift as the decreases in index approach stoichiometric oxide with

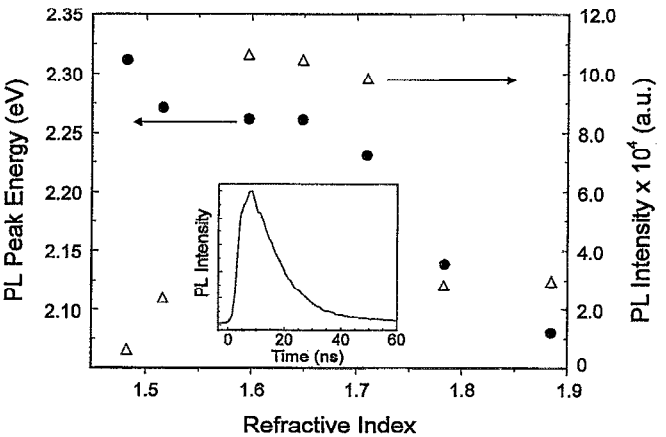

FIG. 3. PL peak energy and intensity vs refractive index for a-SiO_xN_y:H thin films. PL energy on the left-hand-side axis is indicated by the solid circles, and PL intensity on the right-hand-side axis by the open triangles. All data points were taken with a cw Ar^+-ion laser at 488 nm (2.54 eV) excitation wavelength at room temperature. Inset shows a representative time-resolved PL from sample I-c with a characteristic decay time less than 10 ns. Room-temperature time-resolved PL was excited with a pulsed dye laser at 376 nm (3.28 eV) and measured at 488 nm (2.54 eV) emission.

$N=1.47-0.0i$. In addition, Fig. 3 shows nearly a factor of 10 difference in intensity from the best sample, I-c, with an index close to 1.60, and the extremes of the most silicon-rich sample, I-g (highest index), and the one closest to stoichiometry, I-a (lowest index). We believe that the lower intensity of the emission from the lower-index films, and possibly the saturation in the peak shift with index, is a result of the excitation laser being too low in energy (2.54 eV) to provide above-band-gap excitation ($E_{04}>5$ eV) in all but the most silicon-rich samples, which have an optical gap of ~2.5 eV. Excitation at higher energy produces a blue shift in the PL peak with peak emission up to 3.15 eV when excited by the HeCd line at 3.82 eV. Lower-energy excitation causes the peak to red shift. This dependence of the peak emission energy with excitation energy is shown in Fig. 4. This situation was encountered by Carius *et al.*[12] when studying the large-band-gap SiO_x materials with $x>1.3$. Excitation with the 3.82 eV HeCd laser results in a double-peak emission in several samples. Each of the samples had a low-energy peak at ~2.6 eV, but samples I-e and I-g also had a high-energy peak at greater than 3.0 eV. The low-index samples (I-a,I-c) did not show this behavior. This is surprising considering that the low-index samples have the largest optical band gap, and of all of the samples should display the greatest blue-shifted peaks. In addition to the changes in intensity and peak position, the half-width at half-maximum (HWHM) for these PL bands increases with increasing silicon content, with the increase appearing predominantly on the high-energy side of the PL band. Figure 5 shows that the PL intensity is nearly unchanged from 80 to 300 K.

Time-resolved PL was performed on samples I-a, I-c, I-e, and I-g at room temperature. In each case, the time response of the PL was in the same order of magnitude as the response time of the instrument, suggesting radiative lifetimes below 10 ns. This response time was observed both at the PL peak and on the sides of the PL band at energies

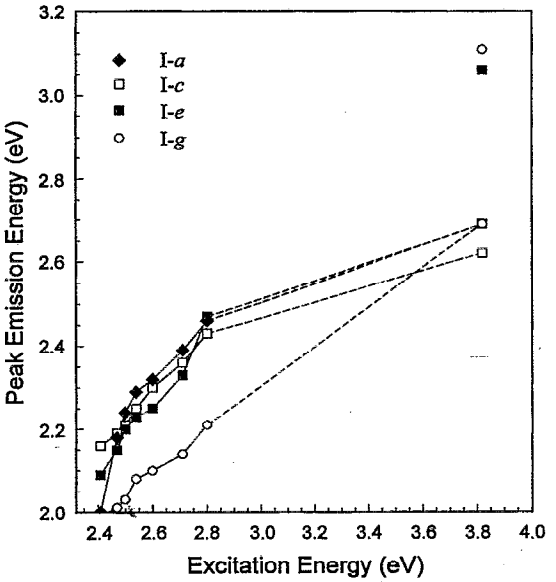

FIG. 4. PL peak emission energy vs laser excitation energy. Excitation was performed at room temperature with the excitation lines from a cw Ar^+-ion laser and a cw HeCd laser. Annealed samples I-(a,c,e,g) are indicated in the legend. The solid lines connect the lower-energy data points, suggesting a blue shift in the peak energy with increasing excitation energy. Excitation with the 325 nm (3.82 eV) line from the HeCd laser resulted in an emission with two distinct peaks for samples I-e and I-g. These are indicated by the separate high-energy points in the top right-hand-side corner. The dashed line connects to the lower energy of the two peaks, suggesting a tentative identification for the 2.6 eV peaks.

greater than half-width (±0.3 eV from peak). A representative transient response is shown in the inset to Fig. 3 for sample I-c at the PL peak. Since the transient response was less than the resolution of the instrument, we were unable to determine the true radiative lifetime, although the decay did not fit a simple single exponential function, and suggests a multicomponent lifetime.

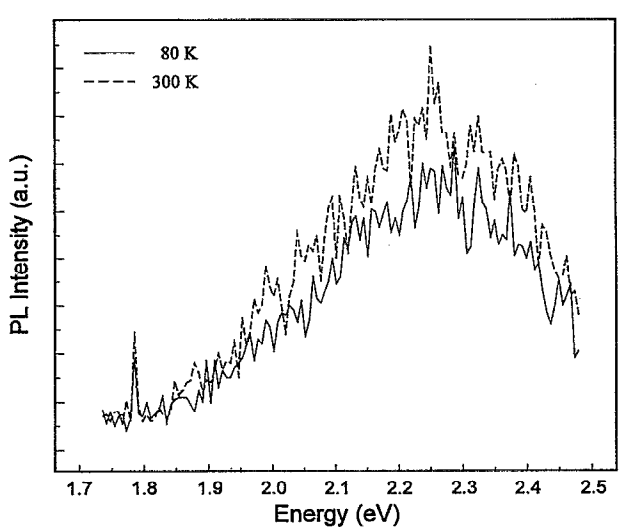

FIG. 5. PL intensity vs energy for sample I-c at room temperature (300 K) and at liquid-N_2 temperature (80 K). The sample was measured after a 30 min anneal in dry N_2 at 1050 °C.

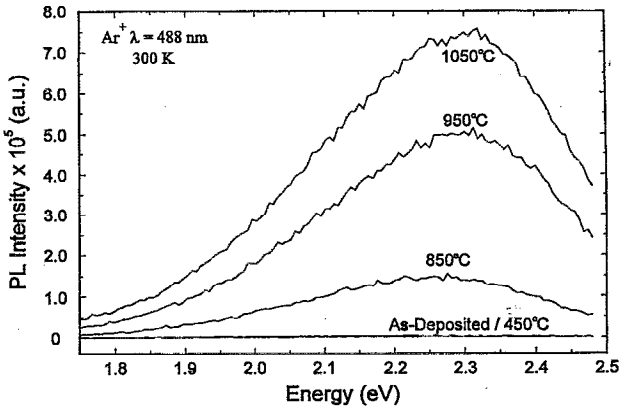

FIG. 6. Isochronal annealing results in terms of PL intensity vs energy for sample II-d for different annealing temperatures. Samples were annealed for 30 min in a dry N_2 ambient, and the spectra were obtained at room temperature.

Sample II-d was used for an atmospheric pressure annealing study to determine if the chemistry of the annealing environment or the annealing conditions of time and temperature affected the PL intensity and energy. Figure 6 demonstrates that there is a dramatic increase in PL intensity with increasing annealing temperature for samples annealed for 30 min in dry N_2. There is also a 0.1 eV blue shift in the peak position with increasing temperature up to saturation at 950 °C. Using identical temperature and time, but in O_2, forming gas, or Ar ambients, there was no difference in the PL intensity or peak position from the samples annealed in a N_2 annealing ambient. In addition, samples annealed in vacuum (2×10^{-7} Torr) also showed no difference in PL intensity or energy when compared to the samples annealed at atmospheric pressure. A study was then performed to determine the effect of annealing time on the PL intensity in a dry N_2 environment. The results can be seen in Fig. 7. At 950 and 1050 °C the PL reaches a saturation value after a 30 min anneal, whereas at 850 °C an 18 h anneal is required in order to reach the saturation value.

There have been literally hundreds of reports of "strong" or "intense" visible PL, without quantification of these adjectives, since the discovery of PL in porous Si. Given the difficulty in defining the quantum efficiency of photoluminescence in solid-state samples, we chose the R emission lines from a ruby sphere as a standard with which to compare the PL efficiency of our films. The quantum efficiency of ruby, defined as the ratio of the radiative recombination rate to the sum of the radiative and nonradiative recombination rates, has been measured to be $QE_R=0.96$ by photothermal[35] and photoacoustic[36] methods. Using the known optical-absorption coefficient of ruby at this wavelength,[37] scaled to the Cr^{3+} concentration in the ruby sphere, together with the measured optical absorption of the film, the absolute quantum efficiency of the film at the 488 nm excitation wavelength was calculated to be 1.12×10^{-4}. This figure is conservative, as the tail of the emission of the film extended beyond the measurement region, and there is some uncertainty in the value of the optical absorption in the

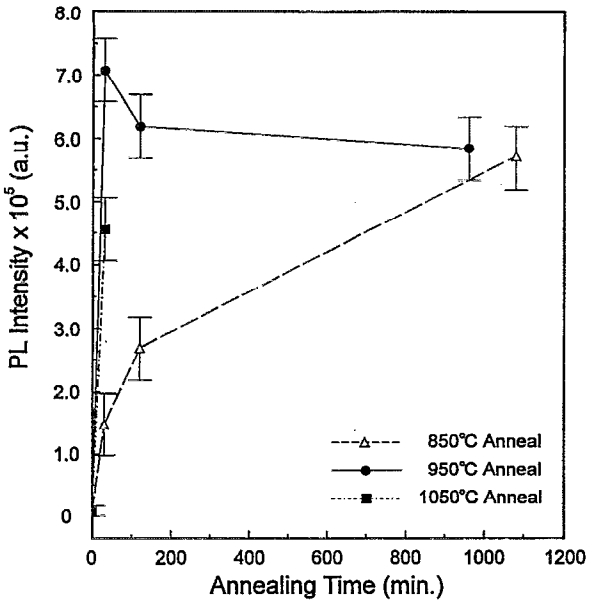

FIG. 7. PL intensity vs annealing time for sample II-d. Samples were annealed in a dry N_2 ambient at the temperatures indicated. The data were obtained with a cw Ar^+-ion laser at 488 nm (2.54 eV) excitation wavelength at room temperature.

films in the low-absorbing region below the optical band gap.

V. DISCUSSION

There are several issues which must be addressed concerning the plasma-deposited oxynitride samples described above in order to understand the optical properties. The most striking feature is the improvement in photoluminescence intensity upon high-temperature annealing. As alluded to earlier, other reports[33,34] suggest that there is an initial increase in PL intensity with increasing annealing temperature, followed by a rapid decrease in intensity at temperatures above 500 °C. One suggestion[33] for the decreasing PL is that the high-temperature annealing produces H_2 evolution from the a-SiN_x:H network, which results in dangling bond states that act as nonradiative recombination centers, and hence lower the radiative efficiency for the annealed samples. This result was compared with a-Si:H, by noting that this same effect is observed at much lower annealing temperatures (~300 °C), and in fact the luminescence is completely quenched at annealing temperatures above 500 °C in a-Si:H. In the more recent study,[34] PL intensity is increased by nearly a factor of 5 with annealing at temperatures up to 500 °C in a-SiO_x:H materials with an accompanying increase in an IR-active absorption mode at 880 cm^{-1}. Annealing temperatures above 500 °C cause a decrease in the PL intensity and a corresponding decrease in the 880 cm^{-1} IR absorption. This IR-absorption mode is attributed to Si–O–Si vibrations in a $(SiO)_n$ ring configuration, which they suggest is evidence of aSi_6-ring structure responsible for the PL.[38] Neither explanation is satisfactory to explain the continued increase in PL intensity at temperatures up to 1050 °C in the present study, and strongly suggests that our material, while containing the same atomic constituents, must have a different microstructure. These temperatures should be more than sufficient to release H_2 from the oxide network, generate dangling bonds, and thus quench the luminescence through the resulting nonradiative centers. The first study, by Fang *et al.*,[33] differs considerably from this result, in that the PL measurements were performed at temperatures as low as 35 K, while in the present study there is almost no temperature dependence on the PL intensity as was shown in Fig. 5. In addition, there is no clear evidence for the 880 cm^{-1} IR absorption present in either the as-deposited or annealed samples shown in Fig. 1. Sample II-b does have a shoulder on the asymmetric stretching resonance at about 870 cm^{-1}, but this is present both as deposited and after annealing, and does not correlate with PL intensity. This is not to say that for annealing at temperatures less than 500 °C this resonance would not be present, but it does suggest that the $(SiO)_n$ chemical species identified by Zacharias *et al.*[34] is not responsible for the efficient luminescence in our materials.

Another observed feature is the lack of phase separation even in the high-refractive-index samples after annealing. This is evident from the amorphous signature in the TEM study, and the lack of two distinct peaks at ~99 and 103 eV in the Si $2p$ region in the XPS study. This behavior is surprising considering that the silicon suboxide moiety is thermodynamically unstable at high temperatures, and other studies on similar CVD materials[17,23,30,31] show separation into nc-Si and SiO_2 after annealing at temperatures above 800 °C. The phase separation reaction can only occur, however, in materials in which the excess silicon is "clustered," or at least atomically close as deposited. The diffusivity of atomic Si in an SiO_2 matrix is small, with a reported value of 8.6×10^{-17} cm^2/s at 1060 °C.[39] This implies that phase separation and recrystallization occur predominantly by nearest-neighbor Si atoms and O diffusion, rather than long-range diffusional rearrangement of silicon atoms in the suboxide matrix in this annealing time scale. We speculate that the presence of Si—N bonds in a relatively high concentration (up to 30 at. %) results in a steric or topological hindrance to the phase separation reaction. The threefold coordinated N may thermodynamically stabilize the suboxide matrix and prevent the phase separation. This process could occur at relatively low excess Si concentrations, as is present here, but we believe that as the volume fraction of silicon continues to increase, ultimately the Si will recrystallize into nc-Si in a SiO_xN_y:H matrix. We are continuing to explore the more silicon-rich phase region in this material.

Two important observations concerning the annealing behavior of this material have been made. The first is that the PL intensity is independent of the annealing ambient. This suggests that the PL is an intrinsic property of the thin films and not the result of new chemistry occurring during the annealing process. This is especially important considering that both O_2 and H_2 annealing ambients should be chemically reactive. The O_2 ambient should result in continued oxidation of the suboxide lattice,[23] and H_2 annealing may result in dangling bond or trap-state passivation, as is common from the microelectronics postmetallization anneal.[40] In both cases, there was no evidence for a change in either PL intensity or peak energy. Interestingly, O_2 annealing did not

appear to oxidize the suboxide lattice in the most silicon-rich sample. This was evident from the lack of change in the refractive index or thickness of sample I-g after a 1.75 h dry oxidation at 950 °C. Si—N bonding is known to be a diffusion barrier to prevent continued oxidation of either the suboxide lattice or the silicon wafer surface.[41]

The second observation is the time-dependent annealing behavior of the films. Figure 7 shows that after only 30 min, annealing at 950 and 1050 °C results in a saturation in PL intensity, while annealing for longer than 10 h is required at 850 °C. There are two straightforward explanations for this behavior. The first is that the process leading to the intense PL is due to diffusion within the thin films, and the second is that local chemistry is responsible for the PL. From the spectroscopic results of Sec. III, it is clear that there are not large changes in the materials before and after annealing. There is some evidence for changes in the bonded Si–H concentration, but overall the bulk properties of the materials seem quite similar before and after annealing. The annealing does not appear to introduce any new chemical bonding configurations in the films which could be attributed to radiative states as Zacharias *et al.* reported.[34] We conclude that the primary result of annealing is the reduction in defect density. As deposited from the plasma, the materials likely contain high bond defect concentrations, which are "healed" upon annealing, allowing radiative recombination to dominate. We have not shown PL results in the IR region, but have observed PL at 0.9 eV which has been attributed to radiative recombination at deep-level dangling bond states.[42] We are continuing to investigate this theory with electron paramagnetic resonance (EPR), and to further examine the time-dependent annealing behavior with a systematic rapid thermal annealing study.

Since the discovery of intense PL for PSi, there have been several reports of blue/green luminescence in the 2.3–2.7 eV energy range in strongly oxidized porous silicon and nanocrystalline-silicon-based materials.[43–47] This has been referred to as the "fast" luminescence band in porous silicon because of the characteristic 1–10 ns lifetime compared to 10 μs lifetime for the red luminescence band in as-anodized porous silicon at room temperature. The transition from the red to blue/green band is not characterized by a monotonic change in the energy of the band, as one would expect from the quantum confinement model of luminescence,[4] but rather by two discrete energy regimes. In addition to blue/green PL in PSi and nc-Si materials, green PL is reported in the a-Si alloys a-SiO_x:H,[12,34] a-SiN_x:H,[13] and a-SiC_x:H,[14] for a high enough x. In most of these materials, the properties such as PL energy, peak width, intensity, temperature dependence, and radiative lifetime are similar, suggesting that the luminescent species is related. While the explanations given to account for the blue/green PL in these materials do not necessarily account for the PL observed in our material, it is remarkable that many of the characteristics of the luminescence behavior are similar despite different preparation conditions. Electrochemical oxidation, PECVD, spark processing,[48] and rapid thermal oxidation should result in vastly different chemistry and morphology. Yet despite these differences, the PL characteristics are unmistakably similar.

The most obvious difference between our SiO_xN_y:H materials and other silicon-based materials is the presence of Si—N bonding. It does not appear to be necessary to have N present in the films in order to realize efficient luminescence. However, as discussed above, the N appears to prevent phase separation and further oxidation of the suboxide moiety thus enabling the material to withstand the high-temperature processing necessary to remove bond defects. In addition, the intensity of the PL does not correlate with the concentration of N present. Chemically, this leaves several similarities to the other materials. Each has the presence of Si—Si, Si—H, and Si—O bonding.

Tamura *et al.*[43] have suggested that the blue/green PL is due to the presence of silanol group Si–O–H adsorbed on structural defects in the silica network. This explanation is not applicable to our results, considering the high annealing temperatures employed here, and the lack of FTIR resonances for the O—H bonding which should be present in Fig. 1(b) in the 3400–3700 cm^{-1} frequency range after annealing. Annealing temperatures greater than 450 °C result in a strong decrease in the silanol coverage, with complete dehydrogenation occurring at temperatures around 1000 °C. Figure 6 shows virtually opposite results, with the PL intensity after annealing at 450 °C being the weakest.

Another possible model is direct band-to-band recombination in silicon nanocrystals due to quantum confinement.[4] Since we do not have crystalline domains of Si, we do not discuss this model further. Also, Tsybeskov and co-workers[47] have shown that this model does not adequately describe the blue emission behavior in oxidized PSi. This same reasoning also excludes the "surface-states" model proposed by Koch.[16] Several other mechanistic possibilities exist, namely emission from the oxide[49] and emission which is characteristic of amorphous silicon-type materials.

It has been shown[49] that SiO_2 exhibits luminescence in a similar energy region with excitation at 6.4 and 7.9 eV. This is below the band gap in SiO_2(~9 eV), yet the luminescence has been attributed to direct excitation of the defect structure in SiO_2. While our excitation energy is far below the band gap in stoichiometric SiO_2, we have shown that the predominant bonding configuration in these thin films is due to SiO_x. Depending on the chemical composition in the films, the band gap in the suboxide material is considerably smaller than 9 eV, and the defect states may be accessible with lower-energy 3–4 eV excitation. The fast transient response in this material (sub-10 ns) suggests that the recombination is due to geminate carriers. Directly accessed luminescent states in SiO_x would be highly localized due to the large potential energy barrier. Statistically, excess carriers would not be able to either demonstrate "hopping" or tunneling to other radiative or nonradiative centers. Since the electron and hole are highly localized, the wave-function overlap would remain strong and allow for radiative recombination. This model also explains the lack of temperature dependence on the PL intensity. The highly localized nature of SiO_x defect sites would prevent tunneling of either the electron or hole to deep nonradiative dangling bond centers near midgap. The highest index samples may exhibit lower radiative efficiency because the defect density is higher and, hence, the probabil-

ity for carriers tunneling to defect states is higher.

Finally, we consider the possibility that the luminescence is the same as that reported for a-Si–based alloys.[50] A primary characteristic of PL in a-Si alloy systems is a monotonic blue shift in the peak position with increasing alloy concentration. This has been attributed to an increasing band gap, and several reports have correlated the change in the optical gap with the change in PL peak energy.[12,13,14,50] This is not the case with our materials. While the refractive index, and, hence, the optical gap, is continuously varied from nearly stoichiometric SiO_2 to SiO, there appears to be a saturation in the peak position of the PL when irradiated by the higher-energy excitation from the 3.82 eV HeCd laser. Even more compelling is that the samples with the smallest optical gap (highest index) all showed a high-energy PL emission at 3.1 eV, while the larger-band-gap materials did not have this high-energy peak. In addition, the 3.1 eV emission is larger than the bulk E_{04} optical gap for sample I-g. Again, this suggests that the luminescence is not due to the band structure in the material, but rather to the defect structure in the suboxide.

Although the results suggest emission due to the defect structure in the silicon suboxide moiety, we have not proposed any specific chemical species for the luminescence. A suggestion posed by Veprek[51,52] appears relevant, namely, that there are hundreds of known organosilane chemical compounds in the literature, most of which luminesce in the blue/green spectral region, and any one of which could be responsible for the luminescence. Most of these have radiative lifetimes on the order of ns, have broad FWHM, and are chemically stable. While we have not experimentally demonstrated this hypothesis, it suggests that the defect structure and/or the bonding at an atomic level introduces radiative states in this material and is responsible for the luminescent behavior in this class of silicon-based materials.

VI. CONCLUSIONS

Since the discovery of light emission from porous Si in 1990 there have been hundreds of reports of intense visible light emission from silicon-based materials. The possibility of a silicon-based technology for optoelectronics has fueled these studies. While many groups have identified the emission, the mechanism is still unclear. Further clouding the issue is the relationship between the emission mechanisms in the different materials; oxidized porous silicon versus silicon nanocrystallites versus amorphous silicon alloys. Yet, the PL energies, peak width, and radiative lifetimes are remarkably similar in each of these distinct materials.

We report the first observation of increasing PL efficiency with increasing annealing temperature in a-Si:H alloy materials. It appears that N is not the radiative center in the SiO_xN_y matrix, but that it may both play a role in providing thermal stability and act as a diffusion barrier enabling the high radiative efficiency after annealing. We have not identified any specific chemical species responsible for the luminescence, but our combined results strongly suggest that the silicon suboxide bonding provides a defect structure which enables visible luminescence.

ACKNOWLEDGMENTS

The authors would like to acknowledge the helpful discussions and input on the manuscript from Dr. D. Han at UNC Department of Physics and Dr. D. Venables at NCSU Department of Materials Science and Engineering. We would like to acknowledge the XPS work performed by W. Ou, and the FTIR work performed by L. J. Richwine and M. L. Clapp at UNC Department of Chemistry. Finally, we would like to thank J. C. Chervin for providing the ruby sphere used in the quantum efficiency measurement, and E. T. Danielson and T. J. Meyer at the UNC Department of Chemistry for the use of the time-resolved PL equipment and software. This research is supported in part by the National Science Foundation (NSF) Engineering Research Center at North Carolina State University.

[1] U. Knutzmann and K. Clausecker, Appl. Phys. **3**, 9 (1974).
[2] J. P. Noel, N. L. Rowell, D. C. Houghton, and D. D. Perovic, Appl. Phys. Lett. **57**, 1037 (1990).
[3] H. Ennen, G. Pomrenke, A. Axmann, K. Eisle, W. Hadyl, and J. Schneider, Appl. Phys. Lett. **46**, 381 (1985).
[4] L. T. Canham, Appl. Phys. Lett. **57**, 1046 (1990).
[5] K. A. Littau, P. F. Szajowski, A. J. Muller, A. R. Kortan, and L. E. Brus, J. Chem. Phys. **97**, 1224 (1993).
[6] M. Rückschloss, B. Landkammer, and S. Veprek, Appl. Phys. Lett. **63**, 1474 (1993).
[7] S. H. Risbud, L. C. Liu, and J. F. Shackelford, Appl. Phys. Lett. **63**, 1649 (1993).
[8] X. Zhao, O. Schoenfeld, J. Kusamo, Y. Aoyagi, and T. Sugano, Jpn. J. Appl. Phys. Lett. **33**, L649 (1994).
[9] T. Shimizu-Iwayama, K. Fujita, S. Nakao, K. Saitoh, T. Fujita, and N. Itoh, J. Appl. Phys. **75**, 7779 (1994).
[10] R. A. Street, J. C. Knights, and D. K. Beigelsen, Phys Rev. B **18**, 1880 (1978).
[11] R. A. Street and J. C. Knights, Philos. Mag. B **42**, 551 (1980).
[12] R. Carius, R. Fischer, E. Holzenkämpfer, and J. Stuke, J. Appl. Phys. **52**, 4241 (1981).
[13] I. G. Austin, W. A. Jackson, T. M. Searle, and P. B. Bhat, Philos. Mag. B **52**, 271 (1985).
[14] L. R. Tessler and I. Solomon (to be published).
[15] W. B. Jackson and R. J. Nemanich, J. Non-Cryst. Solids **59&60**, 353 (1983).
[16] F. Koch, Proc. Mater. Res. Soc. **298**, 319 (1993).
[17] D. Dong, E. A. Irene, and D. R. Young, J. Electrochem. Soc. **125**, 819 (1978).
[18] D. A. G. Bruggeman, Ann. Phys. (Leipzig) **24**, 636 (1935).
[19] D. E. Aspnes, Thin Solid Films **89**, 249 (1982).
[20] Two-step cleaning with $NH_4OH:H_2O_2:H_2O$ (1:1:5) and $HCl:H_2O_2:H_2O$ (1:1:5) each at 65–70 °C in an ultrasonic bath for 5 min. Rinsing and solutions use de-ionized water at 11–13 MW cm resistivity.
[21] H. R. Philipp, J. Phys. Chem. Solids **32**, 1935 (1971).
[22] S. S. Chao, G. Lucovsky, S. Y. Lin, C. K. Wong, P. D. Richard, D. V. Tsu, Y. Takagi, J. E. Keem, J. E. Tyler, and P. Pai, J. Non-Cryst. Solids **77&78**, 929 (1985).
[23] F. Rochet, G. Dufar, H. Roulet, B. Pelloie, J. Perrière, E. Fogarassy, A. Slaoui, and M. Froment, Phys. Rev. B **37**, 6468 (1988).
[24] D. V. Tsu, G. Lucovsky, M. J. Mantini, and S. S. Chao, J. Vac. Sci. Technol. A **5**, 1998 (1987).
[25] G. Lucovsky, J. Yang, S. S. Chao, J. E. Tyler, and W. Czubatyj, Phys. Rev. B **28**, 3225 (1983).
[26] G. Schulze and M. Henzler, Surf. Sci. **124**, 336 (1983).
[27] P. G. Pai, S. S. Chao, Y. Takagi, and G. Lucovsky, J. Vac. Sci. Technol. A **4**, 689 (1986).
[28] G. Lucovsky, P. D. Richard, D. V. Tsu, S. Y. Lin, and R. J. Markunas, J. Vac. Sci. Technol. A **4**, 681 (1986).
[29] P. Swift, Surf. Interface Anal. **4**, 47 (1982).
[30] J. R. Hollahan, J. Electrochem. Soc. **126**, 930 (1979).
[31] P. Pan, L. A. Nesbit, R. W. Douse, and R. T. Gleason, J. Electrochem. Soc. **132**, 2012 (1985).
[32] H. R. Philipp, J. Electrochem. Soc. **120**, 295 (1973).

[33] R. C. Fang, Y. Z. Song, M. Yang, and W. D. Jiang, J. Non-Cryst. Solids **77&78**, 913 (1985).
[34] M. Zacharias, H. Freistedt, F. Stolze, T. P. Drüsedau, M. Rosenbauer, and M. Stutzmann, J. Non-Cryst. Solids **164-166**, 1089 (1993).
[35] A. Mandelis, M. Munidasa, and A. Othonos, IEEE J. Quantum Electron **QE-29**, 1498 (1993).
[36] R. S. Quimby and W. M. Yen, J. Appl. Phys. **51**, 1780 (1980).
[37] W. M. Fairbank, Jr., G. K. Klauminzer, and A. L. Schawlow, Phys. Rev. B **11**, 60 (1975); T. H. Maiman, R. H. Hoskins, I. J. D'Haeneus, C. K. Asawa, and V. Evtuhov, Phys. Rev. **123**, 1151 (1961).
[38] H. Kriegmann, Z. Anorg. Allg. Chem. **298**, 232 (1959).
[39] L. A. Nesbit, Appl. Phys. Lett. **46**, 38 (1985).
[40] E. H. Nicollian and J. R. Brews, *MOS Physics and Technology* (Wiley, New York, 1982), p. 782.
[41] S. Wolf and R. N. Tauber, *Silicon Processing for the VLSI Era* (Lattice, Sunset Beach, CA, 1986), Vol. 1, p. 210.
[42] R. A. Street, Adv. Phys. **30**, 593 (1981).
[43] H. Tamura, M. Rückschloss, T. Wirschem, and S. Veprek, Appl. Phys. Lett. **65**, 1537 (1994).
[44] D. I. Kovalev, I. E. Yaroshetzkii, T. Muschik, V. Petrova-Koch, and F. Koch, Appl. Phys. Lett. **64**, 214 (1994).
[45] T. Ito, T. Ohta, and A. Hiraki, Jpn. J. Appl. Phys. **31**, L1 (1992).
[46] X. Y. Hou, G. Shi, W. Wang, F. L. Zhang, P. H. Hao, D. M. Huang, and X. Wang, Appl. Phys. Lett. **62**, 1097 (1992).
[47] L. Tsybeskov, J. V. Vandyshev, and P. M. Fauchet, Phys. Rev. B **49**, 7821 (1994).
[48] R. E. Hummel and S.-S. Chang, Appl. Phys. Lett. **61**, 1965 (1992).
[49] J. H. Stathis and M. A. Kastner, Phys. Rev. B **32**, 1935 (1987).
[50] T. M. Searle and W. A. Jackson, Philos. Mag. B **60**, 237 (1989).
[51] S. Veprek, in Proc. Mater. Res. Soc., Fall Meeting 1994, Boston, MA (to be published).
[52] See, for example, S. Kyushin, H. Matsumoto, Y. Kanemitsu, and M. Goto, J. Phys. Soc. Jpn. **63**, 46 (1994).